

1 Experimental Design

2 1.1 Boundary Conditions

3 The control and treatment experiments were conducted in the Tulane Sediment Dy-
 4 namics laboratory. The control experiment was conducted in the delta basin in 2018 and
 5 the treatment experiment was conducted in the deep water basin in 2019. Both the con-
 6 trol and treatment experiments had the exact same boundary conditions, except the treat-
 7 ment experiment had marsh deposition and the control experiment did not (Table 1).
 8 Thus, any changes between the two experiments can be attributed directly to the ad-
 9 dition of the marsh.

Table 1: Experiment boundary conditions. The experimental conditions for both the con-
 trol (no marsh) and treatment (marsh deposition) experiments used for comparison in this
 study.

Boundary Condition	Control	Treatment
Sediment Mixture	Hoyal and Sheets (2009)	Hoyal and Sheets (2009)
Realtive Sea Level Rise (RSLR _b)	0.25 mm/hr	0.25 mm/hr
Riverine Sediment Discharge (Q _s)	1.41 kg/hr	1.41 kg/hr
Riverine Water Discharge (Q _w)	1.72*10 ⁻⁴ m ³ /s	1.72*10 ⁻⁴ m ³ /s
In-situ Marsh Deposition (Q _m)	None	150 g/hr (total) 3.7 g/hex (max production) 1.7 g/hex (stable/unstable)

10 1.2 Data and Marsh Proxy

11 We expand here on details of the data collection and marsh distribution. Because
 12 the treatment experiment was not fully automated, we paused the experiment for ~10
 13 hours each night. During the progradation phase, overnight subsidence was tested by tak-
 14 ing a LiDAR scan at the end of the day and beginning of the next day to observe changes
 15 in elevation. No detectable subsidence was observed when the experiments were paused
 16 overnight, thus pausing of the experiment did not impact the elevation data collected
 17 in comparison to the control.

18 We deposited the marsh sediment with about 50% accuracy. An average of 200 g
 19 of kaolinite was deposited per deposition hour, which is less than the average ideal de-
 20 position rate (calculated via the model) of 260 g per deposition (main text Figure 1d).
 21 The reasons for this were (1) compaction of the kaolinite in the sieve and (2) dampen-
 22 ing of the ButtKickerTM signal that caused apparent uneven deposition through time.
 23 We mitigated this by switching the direction of the deposition every two hours (e.g., the
 24 first hour the sieve moved from left to right across the basin to deposit marsh and the
 25 second hour the sieve moved from right to left). We also re-calibrated the sediment dis-
 26 penser after each depositional cycle. Though less accurate than anticipated, the depo-
 27 sition of marsh proxy altered the morphology and surface processes of the delta.

28 **2 Deltaic sediment balance**

29 We calculate the sediment volume balance for both the control and treatment ex-
30 periments in order to directly compare the volume and rate of sediment storage through-
31 out the delta. While this comparison is revealing, we are specifically interested in the
32 influence of marsh sedimentation on delta volume balance; thus, we need to quantify the
33 volume of the riverine and marsh sediment (kaolinite clay) in the treatment experiment
34 throughout its entirety. Due to compaction of the marsh sediment, erosion, and depo-
35 sition of both marsh and river sediment in the same area on the delta top, we cannot
36 directly quantify the sediment accumulation using the LiDAR scans. Instead, we take
37 advantage of the preserved stratigraphy to determine the marsh volume.

38 **2.1 Stratigraphic Interpolation**

39 The resulting stratigraphy was split into two sections to acquire one cross-section
40 along dip. Then the deposit was sectioned from distal to proximal along strike every 10
41 cm. Photographs were taken of each section and color image processing was used to ob-
42 tain a marsh fraction and thickness roughly every 10 cm (Figure 1a).

43 Using this gridded stratigraphic data, we use Bayesian kriging techniques (“Bayesian
44 inference”, 2007) to interpolate a pixel (5 mm x 5 mm) marsh fraction and marsh thick-
45 ness for the entire delta basin (Figure 1b and c). Bayesian kriging is a useful interpo-
46 lation technique because it integrates data and model to predict values and uncertainty
47 on those predicted values (“Bayesian inference”, 2007). Further, it is less likely to be bi-
48 ased than traditional interpolation techniques, producing a more accurate model (“Bayesian
49 inference”, 2007).

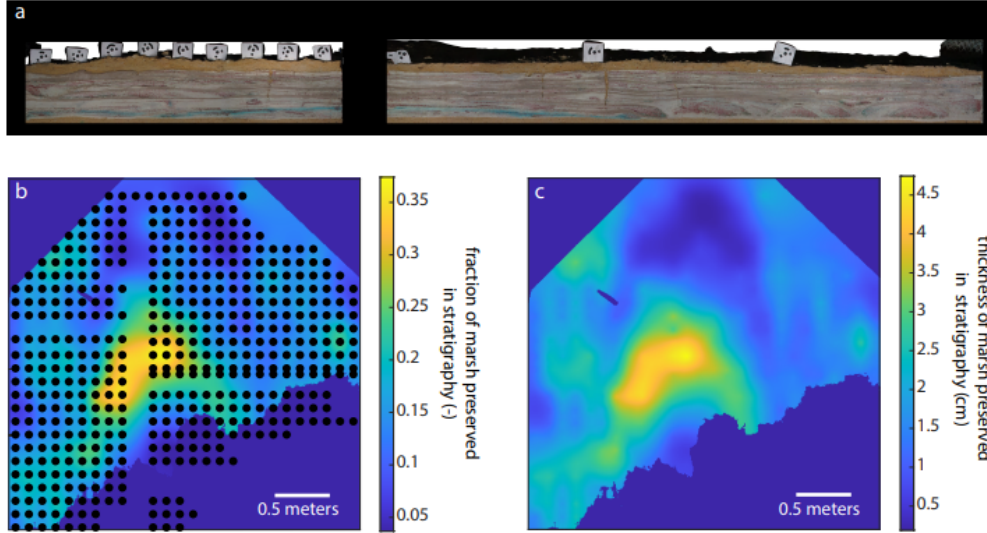


Figure 1: Stratigraphic Interpolation. (a) An along strike section of the treatment experiment at 1.1 m from the entrance channel. The targets on the left one-third of the image are spaced 10 cm apart and thickness and fraction of marsh was collected for the entire deposit below each target. The red sediment is channel sand, white is channel floodplain, and brown is marsh. The tan sediment above and below the section is play sand and not part of the delta deposit. (b) The interpolated fraction of marsh sediment that is preserved in stratigraphy for the area above -9 mm relative to seal level for at least 10% of the experiment. The black dots represent the measured values of marsh fraction and thickness and are roughly 10 cm apart. The raw data (black dots) was interpolated using a 5 mm x 5 mm grid (the resolution of the LiDAR data). (c) The interpolated thickness of marsh sediment that is preserved in the stratigraphy (cm) using a 5 mm x 5 mm grid.

50

2.2 Volume Balance

51

52

53

54

55

56

57

58

59

60

The volume balance for the different zones (e.g., above marsh, marsh window, delta top) was calculated using the final resulting stratigraphy. We define the region above the marsh as the area that is above 5 mm relative to sea level (rsl) for at least 90% of the experiment to minimize the influence of marsh on sedimentation of this region in the treatment experiment. The marsh window is the area ≤ 5 mm rsl and ≥ -9 mm rsl for greater than 10% of the experiment. By using this criteria, the marsh window begins exactly where the above marsh zone ends. Finally, we define the delta top as the area that is ≥ -9 mm rsl for at least 50% of the experiment. This region then encompasses a smaller extent than the combined above marsh and marsh window area. However, we use this region to compare the average delta top area and volume of the two experiments.

61

62

We calculate the volume balance for all three zones using the following logic. Total sediment accumulated (V_T ; mm^3) at each pixel (i) is given by:

$$V_T = (Z_{\text{final}} - Z_{\text{initial}}) * A_{\text{pixel}}, \quad (1)$$

63

64

65

66

where z_{final} is the pixel elevation of the last LiDAR scan, z_{initial} is the pixel elevation of the first LiDAR scan, and A_{pixel} is the area of one pixel (25 mm^2). From there, we multiply by the interpolated marsh fraction (f_m ; -) to determine the marsh sediment accumulated (V_m ; mm^3), given by:

$$V_m = f_m * V_T. \quad (2)$$

67 The clastic (riverine) sediment accumulated (V_c ; mm^3) is then:

$$V_c = V_T - V_m. \quad (3)$$

68 Note that because the control experiment has no marsh deposition, V_m is 0 and
69 V_c is simply equal to V_T . Refer to Table 1 in the main text for the zonal volume bal-
70 ance.

71 We compared the zonal mass balance for the area above the marsh to a mass bal-
72 ance calculated using a moving average above the marsh window. The moving window
73 shows a sediment accumulation rate of 0.202 m^3 and 0.0655 m^3 for the control and treat-
74 ment experiments, respectively. While this is about a 40% difference from the integrated
75 zonal volume, both methods show a similar percent difference in volume between the two
76 experiments. We integrated through time for each of the three zones (above marsh, marsh,
77 and delta top) because even though the delta is in equilibrium, autogenic variability im-
78 pacts short-term sediment deposition and resulting stratigraphy (i.e., the moving aver-
79 age does not account for long- or short-term compactional subsidence) (Jerolmack & Sadler,
80 2007).

81 The trapping efficiency (TE; %) is defined by:

$$TE = \frac{V_c}{V_D} * 100, \quad (4)$$

82 where V_D (a constant 0.660 m^3) is the clastic sediment delivered to the delta top and
83 calculated by:

$$V_D = \left(\frac{\text{flux}}{\rho} * t \right) * 10^{-6}, \quad (5)$$

84 where flux is the sediment being delivered to the system by the river (a constant 1406.14
85 g/hr), t is the entire run time of the experiment (560 hrs), and ρ is the bulk density of
86 the clastic sediment (a constant 1.19 g/cm^3), assuming an average 55% porosity (mean
87 of cores taken from the control experiment) and a particle density of 2.65 g/cm^3 .

88 In Table 1 of the main text, we calculate two TE for the marsh window. The TE
89 described by footnote a in Table 1 is the TE calculated using the clastic sediment deliv-
90 ered to the marsh window (V_{Dm}) instead of the clastic sediment delivered to the delta
91 top (V_D):

$$V_{Dm} = V_D - V_{am}, \quad (6)$$

92 where V_{am} is the total clastic sediment accumulated above the marsh window.

93 3 Delta Hypsometry

94 We compare the hypsometry (elevation distribution) of the control and treatment
95 experiments to the hypsometry of three vegetated and one non-vegetated field-scale deltas.
96 In order to compare the experimental scale to the field scale, we non-dimensionalize the
97 elevations of the delta top by dividing elevation by one average channel depth for the
98 given system. The channel depths used are 15 mm for the experiments, 30 m for the Mis-
99 sissippi River Delta (MRD) and the Ganges Brahmaputra Meghna Delta (GBMD),
100 10 m for the Mekong River Delta, and 15 m for the Rio Grande River Delta. Notably,
101 we see a more similar hypsometric signature between the treatment and global deltas,
102 as compared to the control. The treatment and global deltas have >30% of their eleva-
103 tions between 0 and 0.5 channel depths above sea level. Specifically, the treatment ex-
104 periment has 31%, MRD has 44%, GBMD has 64%, Mekong River Delta has 50%, and
105 Rio Grande River Delta has 38% of elevations here. Comparatively, the control only has
106 17% of elevations in this 0 to 0.5 channel depths above sea level window. Rather, the
107 control has a bi-modal distribution with peaks at 0.06 channel depths below sea level and
108 0.733 channel depths above sea level.

109 The elevation data for the field scale deltas was collected using ETOPO Global Re-
 110 lief Model (NOAA) in Google Earth Engine (GEE). GEE provides an interactive soft-
 111 ware, which we used to create polygons of the delta tops of three vegetated deltas (the
 112 Mississippi River Delta, Ganges Brahmaputra Meghna Delta, and Mekong River Delta),
 113 and one mostly unvegetated delta (the Rio Grande River Delta) (Figure 2).

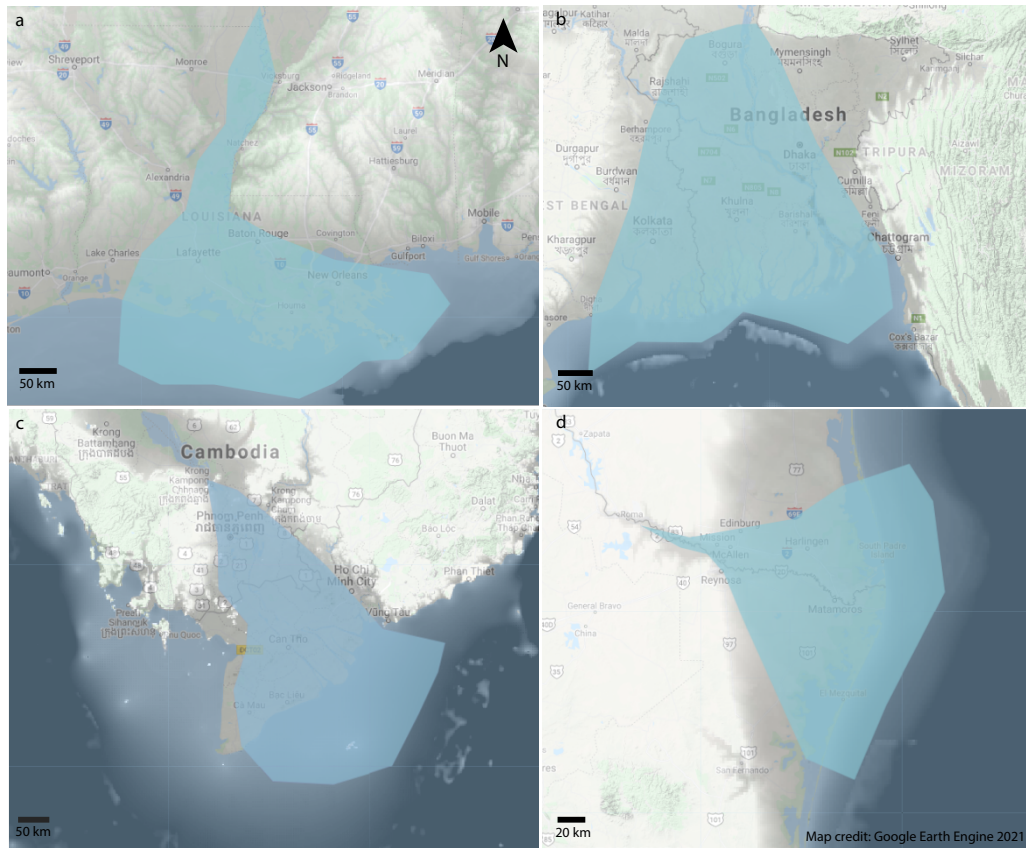


Figure 2: Delta polygons. The satellite and topographic data for the field-scale deltas used in the hypsometric analysis and the corresponding polygons (blue) used to obtain elevation data. (a) The Mississippi River Delta located in Louisiana, USA. (b) The Ganges Brahmaputra Meghna Delta located in Bangladesh and West Bengal, India. (c) The Mekong River Delta located in Cambodia and Vietnam. (d) The Rio Grande River Delta located on the border of southeast Texas, USA and northeast Mexico. The scales vary on each map, but the north arrow and credits are the same for all.

114 The polygons were created with the following rules. (1) We avoided locations that
 115 were greater than 3 channel depths above to sea level and less than 1 channel depth
 116 below sea level, (2) we attempted to determine the entrance of the channel into the “delta
 117 top”, and (3) we made sure to include the main distributary channels within the poly-
 118 gon area. While the areas were chosen somewhat arbitrarily, we tested different poly-
 119 gons for the same delta and did not observe a significant difference in the histogram dis-
 120 tribution shape, thus we are confident in the patterns observed in Figure 4 (main text).

121 **References**

- 122 Bayesian inference. (2007). In P. J. Diggle & P. J. Ribeiro (Eds.), *Model-based*
123 *Geostatistics* (pp. 157–198). New York, NY: Springer. Retrieved 2021-08-22,
124 from https://doi.org/10.1007/978-0-387-48536-2_7 doi: 10.1007/978-0-
125 -387-48536-2_7
- 126 Jerolmack, D. J., & Sadler, P. (2007). Transience and persistence in the deposi-
127 tional record of continental margins. *Journal of Geophysical Research: Earth*
128 *Surface*, 112(F3). Retrieved 2021-10-12, from [https://onlinelibrary.wiley](https://onlinelibrary.wiley.com/doi/abs/10.1029/2006JF000555)
129 [.com/doi/abs/10.1029/2006JF000555](https://onlinelibrary.wiley.com/doi/abs/10.1029/2006JF000555) doi: 10.1029/2006JF000555